

Abstract

Our investigation aimed to analyse the contact pressure distribution, the contact area and the sliding procedure in a railway wheel-rail contact by using finite element method. The analysis were created with linear elastic material model. The elaborated model provides opportunity to analyse the initial sticking zone within the contact zone that disappears and transforms into full sliding contact due to the tangential displacement of the contact zone. In that state we examined the equivalent stress distribution under the surface in full sliding condition as well.

Keywords

contact pressure · Hertzian contact · wheel-rail contact · initial stick slip · full sliding

1 Introduction

The analysis of the railway wheel-rail contact is an important research area in the railway development. This connection has effect on the running comfort, dynamics, the failure of wheel tread and the wear as well.

In the article of Kleiner and Schindler [1] an FE analysis were used to determine the pressure distribution between the two contacting elements. Their analyses involve seventeen contact positions between a S1002 wheel profile and a 60E2 rail profile. They provided an empirical equation, which makes it possible to determine, with a good approximation, the maximum surface pressure depending on the wheel load and the lateral displacement of the wheel relative to the rail.

Telliskivi et al. [2] compared three different methods to determine the contact pressure and the contact area in the wheel-rail connection in different contact cases. They used the traditional Hertzian analytical calculation (when it was valid), the CONTACT software (based on Kalker's theory [3]) and an FE analysis with elastic-plastic material law. They pointed out that the traditional methods only provided accurate results when the minimum contact radius is large compared to the significant dimensions of the contact area (when the half space assumptions is valid).

Wiest et al. [4] created analyses between a railway wheel and a crossing nose with different numerical and analytical methods similarly to Telliskivi et al. They examined and compared the contact area, the contact pressure distribution and the rigid body approach. The results show of the importance of using elastic-plastic analyses for studies of contact stresses.

Zhao et al. [5] examined the wheel-rail contact with a 3D FE model, for a simplified geometry. They analysed the contact pressure distribution, the surface shear stress distribution and adhesion-slip area within the contact zone. The results were compared to CONTACT and analytical Hertz solutions. They pointed out that the created simplified geometry provides reliable solution of frictional rolling contact, in statics and dynamics, in elasticity and plasticity.

Pau et al. [6] examined the wheel-rail contact in a different way. They used ultrasonic method to determine the contact

Péter T. Zwierczyk
Budapest University of Technology and Economics,
Műegyetem rkp. 3., H-1111 Budapest, Hungary
e-mail: z.peter@gt3.bme.hu

Károly Váradi
Budapest University of Technology and Economics,
Műegyetem rkp. 3., H-1111 Budapest, Hungary
e-mail: varadik@eik.bme.hu

pressure between the contacting bodies. With the help of this technique the contact pressure distribution can be analysed if the numerical and analytical techniques are not readily and reliably applicable or it can be used to analyse the rolling contact under the vehicle in motion.

Our goal with the elaborated FE analyses – created with ANSYS V14.5 FE software – is to compare the contact behaviour in a railway wheel-rail contact during, stationary as well as sticking and sliding conditions.

2 The FE model

In the course of our investigations, a 40° piece of a railway wheel of $D=920$ mm [7] diameter and with simplified geometry and a 560 mm long rail, according to the UIC-60 profile standard [8] was examined (Fig. 1.). In the course of calculations, the flange of the wheel rim and the conical shape of the tread were neglected. With a view to the fact that the geometries thus established are totally symmetrical to the Y-Z plane, half models were produced from the pieces extracted for calculations.

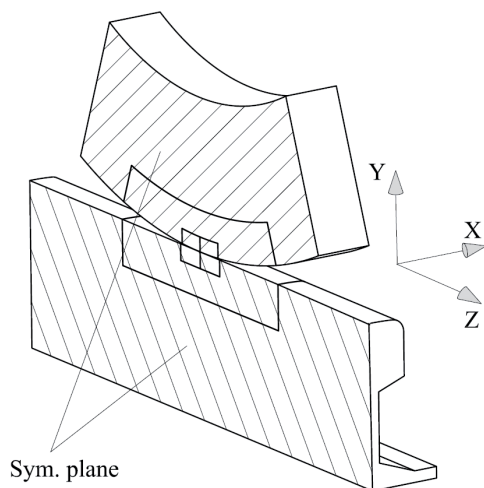


Fig. 1. The structural geometry, with symmetry conditions

The segments of the analyses according to Fig. 1. were broken down into sub-segments. This was intended to produce a sufficiently fine mesh at the places required. The sub-segments are shown in Fig. 2.

A so-called bounded mesh [9] was produced between each segment in order to simplify links and to reduce the number of components, therefore bounded contact relations were defined between mesh segments (Fig. 3.).

For the sake of greater calculation accuracy, 20-node hexahedron elements were used at each segment. In case of the base bodies (C), the element size was 15 mm; in case of segments marked by (B) it was 5 mm; in case of segments marked by (A) it was 0.9 mm. Thus the FE mesh consisted of 57 229 elements and 249 973 nodes for the whole geometry.

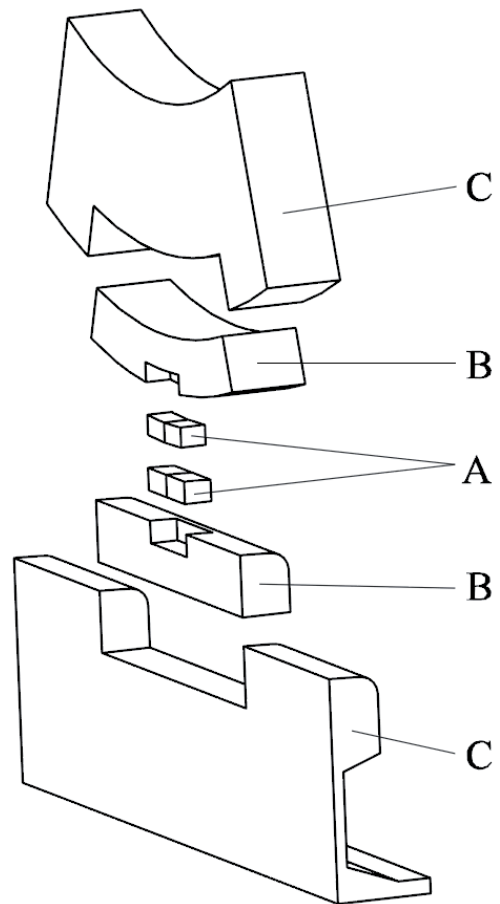


Fig. 2. Structure of the segmented geometry (vertically drawn apart)

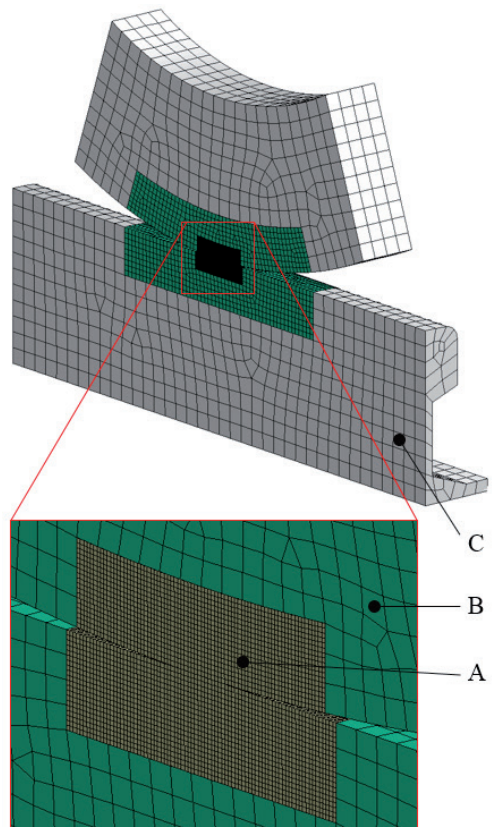


Fig. 3. The structure of the FE mesh

2.1 The material properties

During the analysis we used linear elastic material model for both of the rail and the wheel. The material properties are listed in Table 1. In case of the wheel we assumed SSW-3QS wheel material [10], in case of the rail we used ordinary steel material properties.

Tab. 1. Material properties applied during the analysis at 25°C.

Material:	
Wheel: SSW-3QS according to JIS E 5401 [10] (similarly to the European ER9 steel grade according to the EN13262 standard)	
Rail: generic steel	
Modulus of elasticity [MPa](wheel):	206 000
Modulus of elasticity [MPa] (rail):	200 000
Density [kg/m ³]:	7850
Poisson ratio [-]:	0.3

2.2 Boundary and loading conditions

In the course of calculations, the total weight of the vehicle was ~520 kN [7], representing ~F=63 750 N load per wheel, assuming that the vehicle has four axles. At first frictionless contact was applied between the wheel-rail connection (stationary position), later sliding contact was studied.

We applied fixed boundary condition on the top and the side surfaces of the wheel model to model the stationary contacts (I in Fig. 4.). On the bottom and side surfaces of the rail a prescribed displacement constrain (II) was applied. Initially we fixed the X and Z movement of the rail and a prescribed value of 0.0796 mm in Y direction was applied which provided the necessary loading force according to the Hertz theory [11]. On both of the analysed bodies symmetry constrains (III) were applied along the symmetry planes according to Fig. 1.

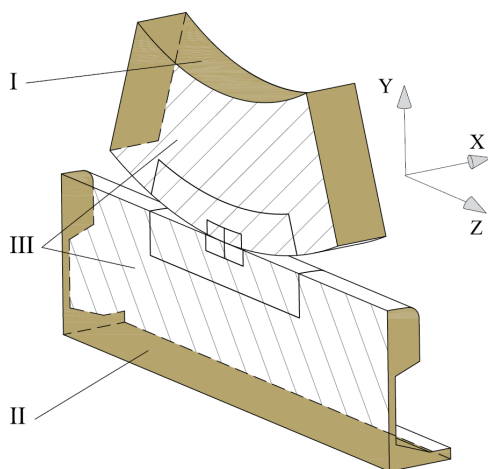


Fig. 4. The applied boundary conditions

3 Results

In the course of calculations, three query lines were specified on the wheel, along which results were queried (we queried the results only on the wheel because of the conformity of the material properties). Fig. 5. shows the location of query lines.

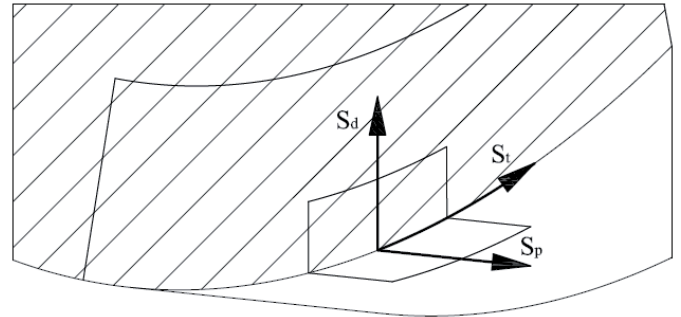


Fig. 5. Location of query lines used for the evaluation of results on the wheel model: St according to the direction of rolling, Sd in the direction of depth, Sp in perpendicularly to the symmetry plane

3.1 Contact pressure distribution

The contact pressure distributions are shown in Fig. 6. It can be seen that the distribution is about symmetric, the diagram shapes are according to the Hertz theory. The maximum pressure value is 1011.4 MPa. Fig. 7. shows the contact stress both of the wheel and the rail near the contact area.

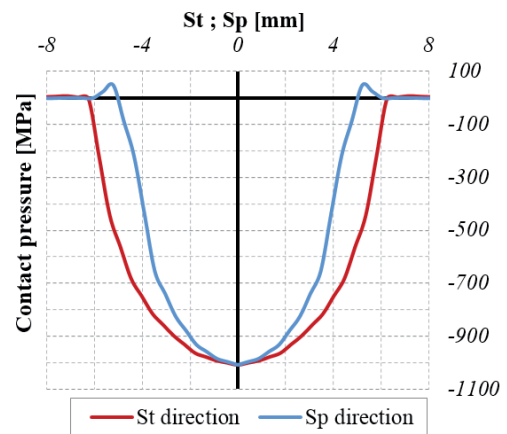


Fig. 6. The contact stress distribution on the wheel

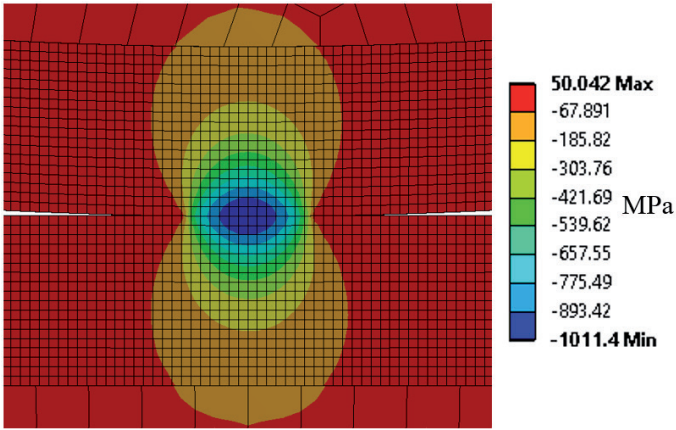


Fig. 7. The s_y normal stress distribution near the contact area

To validate our analyses we prepared an analytical calculation to determine the maximum contact pressure according to the Hertz theory [11]. The maximum values of the contact pressure according to the different calculation methods (analytical and linear elastic FE analysis) are shown in Tab. 2. As it can be seen, the difference is $\sim 2.4\%$ between the maximum contact pressures. In this case the FE analyses are accurate enough.

Tab. 2. The maximum contact pressures

FEM	Analytical
1011.4 MPa	1036.28 MPa

Similarly to the contact pressure, we examined the von Mises equivalent stress distribution along the Sd query line. An overview about the equivalent stress can be seen in Fig. 8. near the contact region. Fig. 9. contains the equivalent stress distribution along the Sd query line.

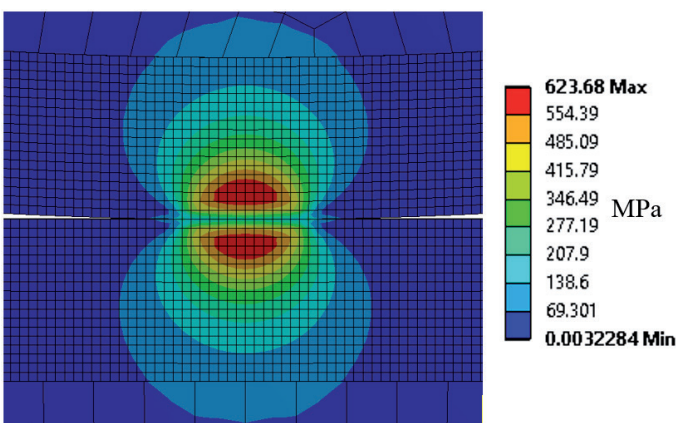


Fig. 8. The von Mises equivalent stress distribution near the contact area

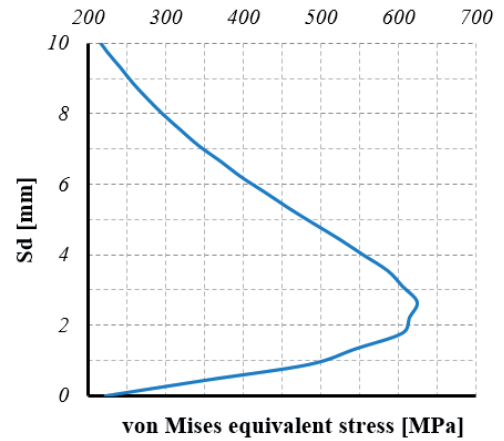


Fig. 9. The equivalent, von Mises stress distribution along the Sd query line on the wheel

The curve gets its maximum in the region of 2-4 mm depth under the running tread. Fig. 10. and Fig. 11. shows the principal shear stress distribution along the Sd query line.

The principal shear stress reaches its maximum under the wheel tread which is conformable with the Hertz theory [12].

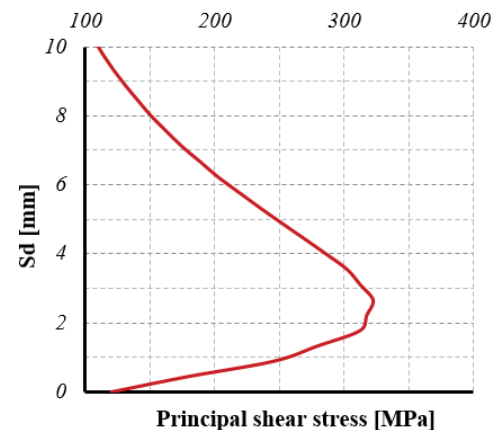


Fig. 10. Principal shear stress distribution along the Sd query line on the wheel

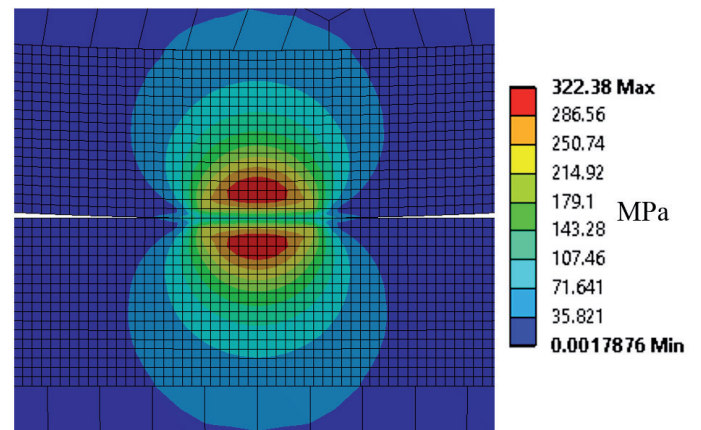


Fig. 11. Principal shear stress distribution near the contact region (in stationary position)

4 The slipping procedure between the wheel and the rail

In the second part of our analysis we examined the slipping procedure of the wheel. To do that the constrain of the wheel has been modified. A prescribed displacement constrain was applied in the wheel which allowed $1.087 \cdot 10^{-5}$ rad rotation (0.005 mm tangential displacement), meanwhile the constrains of the rail were being unchanged (Fig. 12.). In addition $\mu=0.15$ [13] frictional coefficient was applied between the contacting bodies.

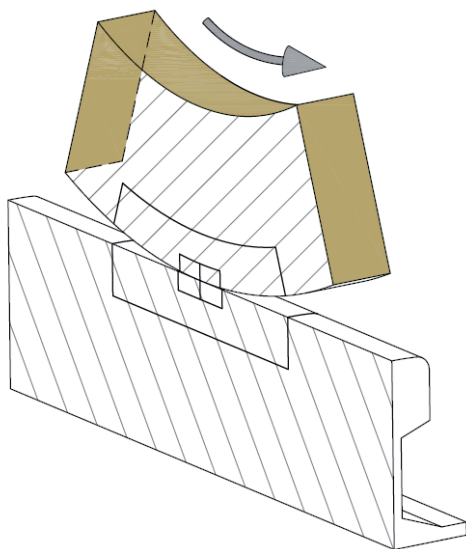


Fig. 12. The modified boundary condition on the wheel

To examine the initial sticking zone within the contact zone we analysed the tangential displacement of the wheel and the rail in the stationary position, at first. In Fig. 13. the sticking zone is nearly the half of the contact zone in the stationary position. Fig. 14-16. show the tangential displacements when the wheel displaced $2.5 \cdot 10^{-4}$ - $7.5 \cdot 10^{-4}$ mm. As it can be seen in the figures the extension of the sticking zone decreased. After that when the sticking zone goes to zero the contacting elements slips in each other. In this case the tangential displacements are independent from each other as it can be seen in Fig. 17. (when the wheel displaces $1.5 \cdot 10^{-3}$ mm).

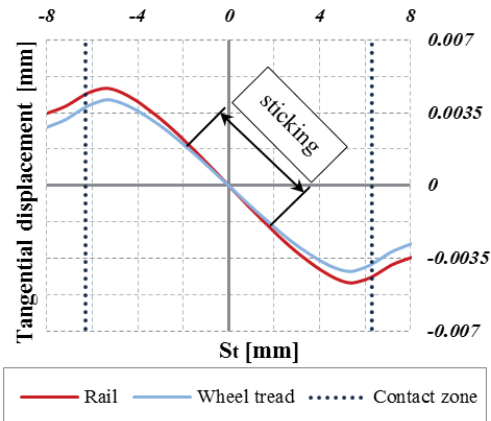


Fig. 13. The tangential displacement of the rail and the wheel, with the sticking zone, at stationary position

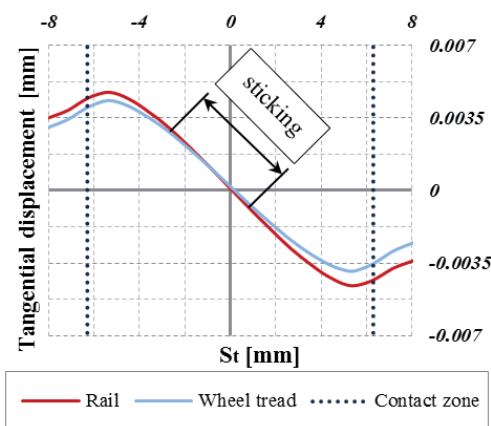


Fig. 14. The tangential displacement of the rail and the wheel still under sticking (wheel displaces $2.5 \cdot 10^{-4}$ mm)

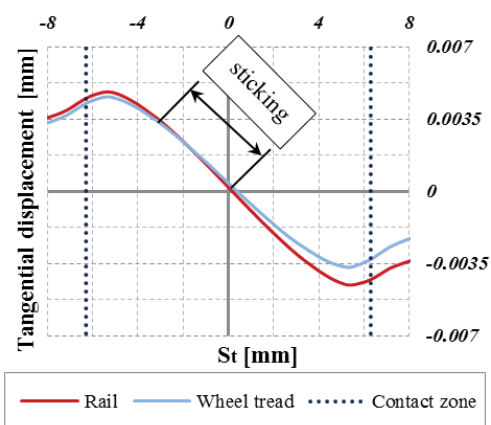


Fig. 15. The tangential displacement of the rail and the wheel still under sticking (wheel displaces $5 \cdot 10^{-4}$ mm)

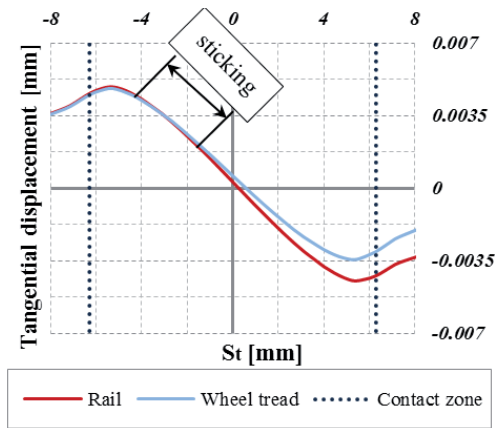


Fig. 16. The tangential displacement of the rail and the wheel still under sticking (wheel displaces $7.5 \cdot 10^{-4}$ mm)

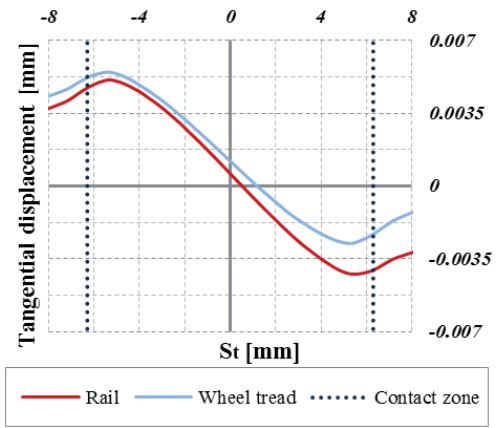


Fig. 17. The tangential displacement of the rail and the wheel (wheel displaces $1.5 \cdot 10^{-3}$ mm)

Beside the tangential displacements we examined the equivalent von Mises stress at the end of the analysis (Fig. 18), showing the effect of friction.

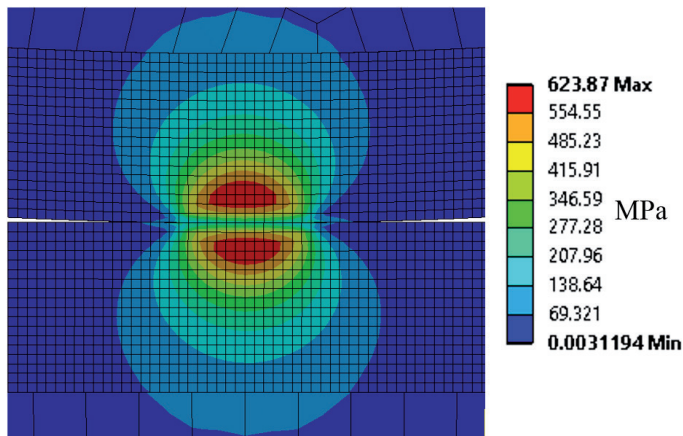


Fig. 18. The equivalent von Mises stress distribution in the vicinity of the contact region (the wheel displaces 0.005 mm)

5 Conclusion

A railway wheel-rail contact was analysed in our work. In the first part of our analysis we examined the contact normal stress distribution between the wheel and the rail and validate it with an analytical Hertz calculation. Beside the contact normal stress we examined the equivalent von Mises stress distribution on and under the contact surfaces as well.

As it can be seen in Figs. 9-11. the maximum of the equivalent von Mises stress and the principal shear stress occurs under the wheel tread in 2-4 mm depth.

In the second part of our analysis we examined the initial stick-slip phenomenon when the wheel slips on the rail. The results show that the initially sticking zone, within the contact zone decreases after only ~ 0.0015 mm tangential displacement of the wheel (Figs. 13-17). The equivalent von Mises stress lost its symmetricity as it can be seen in Fig. 18.

References

- 1 Kleiner O., Schindler C., *Investigating the stress on wheel and rails*. Railway Technology Review, 51 (4), pp. 15–21, (2011).
- 2 Telliskivi T., Olofsson U., Sellgren U., Kruse P., *A tool and a method for FE analysis of wheel and rail interaction*. In: Proc. of ANSYS Conf. Pittsburgh, Pennsylvania, USA (2000).
- 3 Kalker J. J., *Two algorithms for the contact problem in elastostatics*. Proc. Int. Symp. on Contact Mechanics and Wear of Rail-Wheel Systems I. Vancouver BC., pp. 101–120, (1982).
- 4 Wiest M., Kassa E., Daves W., Nielsen J. C. O., Ossberger H., *Assessment of methods for calculating contact pressure in wheel-rail/switch contact*. Wear, 265 (9-10), pp. 1439–1445, (2008). DOI: [10.1016/j.wear.2008.02.039](https://doi.org/10.1016/j.wear.2008.02.039)
- 5 Zhao X., Li Z., *The solution of frictional wheel-rail rolling contact with a 3D transient finite element model: Validation and error analysis*. Wear, 271 (1-2), pp. 444–452, (2011). DOI: [10.1016/j.wear.2010.10.007](https://doi.org/10.1016/j.wear.2010.10.007)
- 6 Pau M., Aymerich F., Ginesu F., *Distribution of contact pressure in wheel-rail contact area*. Wear, 253 (1-2), pp. 265–274, (2002). DOI: [10.1016/S0043-1648\(02\)00112-6](https://doi.org/10.1016/S0043-1648(02)00112-6)
- 7 Siemens Viaggio Classic-emotion@rail, RIC/UIC – Passenger Coach Platform. http://www.mobility.siemens.com/mobility/global/SiteCollectionDocuments/en/railsolutions/passenger-oaches/Viaggio_Classic_4Seiter_en.pdf, (date of download: 02.13.2013.)

- 8 **DIN EN 13674-1**, *Railway applications – Track – Rails, Part 1: Vignole railway rails $\geq 46\text{kg/m}$*
- 9 *Ansys V14.5 Program Help* (2012).
- 10 **Handa K., Morimoto F.**, *Influence of wheel/rail tangential traction force on thermal cracking of railway wheels*. *Wear*, 289, pp. 112-118 (2012).
DOI: [10.1016/j.wear.2012.04.008](https://doi.org/10.1016/j.wear.2012.04.008)
- 11 **Mutnyánszky Á.**, *Szilárdságtan*. Műszaki Könyvkiadó, Budapest (1981). (in Hungarian)
- 12 **Johnson K. L.**, *Contact mechanics*. Cambridge University Press, Cambridge (1984).
- 13 **Kragelszkij I. V., Vinogradova I. E.**, *A súrlódási tényező*. Műszaki Könyvkiadó, Budapest (1961). (in Hungarian)